Acta Materialia 101 (2015) 55–61

Contents lists available at ScienceDirect

Acta Materialia

journal homepage: www.elsevier.com/locate/actamat

Solid solution hardening of vacancy stabilized $Ti_xW_{1-x}B_2$

H. Euchner [a,*], P.H. Mayrhofer [a], H. Riedl [a], F.F. Klimashin [a], A. Limbeck [b], P. Polcik [c], S. Kolozsvari [c]

[a] Institute of Materials Science and Technology, TU Wien, 1060 Vienna, Austria
[b] Institute of Chemical Technology and Analytics, TU Wien, 1060 Vienna, Austria
[c] Plansee Composite Materials GmbH, 86983 Lechbruck, Germany

ARTICLE INFO

Article history:
Received 25 June 2015
Revised 4 August 2015
Accepted 19 August 2015
Available online 19 September 2015

Keywords:
$Ti_{1-x}W_xB_2$
Sputtering
Vacancies
Density functional theory

ABSTRACT

We present a combined experimental and theoretical investigation of sputter deposited thin films in the ternary system $Ti_{1-x}W_xB_2$. Solid solutions of $Ti_{1-x}W_xB_{2-z}$ were prepared by physical vapor deposition (PVD) and, over the whole composition range, found to crystallize in the AlB_2 structure type. The obtained films exhibit good thermal stability and high hardness, evidencing a maximum value of almost 40 GPa for $Ti_{0.67}W_{0.33}B_{2-z}$. The effect of vacancies on stabilization and mechanical properties of the AlB_2 structure type is discussed, using ab initio simulations. Based on our results, we can conclude that vacancies are crucial for the phase stability of PVD deposited $Ti_{1-x}W_xB_{2-z}$ coatings.

1. Introduction

The increasing industrial demand for protective coatings with high hardness, good elastic properties and thermal stability calls for the investigation of new material systems. Although transition metal (TM) nitrides are successfully applied for different tasks in automotive or aerospace industries, the search for improved materials is an ongoing topic, being far from its end.

It is well known that vapor phase deposition techniques allow the growth of supersaturated solid solutions such as cubic B1 $Ti_{1-x}Al_xN$ (rocksalt structure, NaCl prototype). In case of $Ti_{1-x}Al_xN$, the supersaturation of the TiN-based cubic structure increases with higher Al fractions. At elevated temperatures, this allows for self-hardening effects, resulting from spinodal decomposition and formation of TiN- and AlN-rich cubic domains [1–3]. Only the transition from cubic to wurtzite AlN, which takes place upon further annealing, typically results in a loss of mechanical properties, may, however, due to the enormous volume change, induce a toughening effect for controlled AlN phase fractions [4]. Thus, the unique properties of $Ti_{1-x}Al_xN$ originate from the interplay and competition of two phases, preferring different structure types – cubic TiN and wurtzite AlN.

Making use of the concepts on which the exceptional properties of $Ti_{1-x}Al_xN$ are based, ternary borides have recently been suggested as promising candidates for strong materials with exceptional properties [5]. However, while ternary and even quaternary TM nitrides have been investigated in detail, multinary borides are largely unexplored.

A large number of diborides, including the well-studied and technologically important TiB_2 phase [6–9], prefer the so-called AlB_2 structure type [10] and crystallize in a three atoms unit cell with space group 191 ($P6/mmm$). An instructive description of this structure, as a stacking of hexagonal planes with covalently bonded boron atoms that are separated by metal layers, is given in Fig. 1(a). The boron atoms form graphite-like, covalently bonded hexagons, with metal atoms above (and below) their centers. In addition to the predominant AlB_2 structure type, different structural modifications of diboride phases are known. One such example is WB_2, for which two different modifications are reported [11–14]. Recently, WB_2 thin films were reported to crystallize in the AlB_2 structure, whereas bulk material prefers the WB_2 modification, formerly known as W_2B_5. The WB_2 structure type is closely related to the AlB_2 prototype but evidences a different layer structure, with both flat and puckered boron layers. This results in an increased unit cell, containing twelve atoms and crystallizing in space group 194 ($P63/mmc$) as depicted in Fig. 1(b). For simplification, in the following, the AlB_2 structure will be named α-phase, whereas the WB_2 structure type will be refereed to as ω-phase.

In this work magnetron sputtering has been used to deposit $Ti_{1-x}W_xB_{2-z}$ thin films with varying Ti/W ratio. Interestingly, over the whole composition range, the coatings were found to crystallize in the AlB_2 structure type. The films show high hardness, with a maximum value of almost 40 GPa in case of $Ti_{0.67}W_{0.33}B_{2-z}$. Moreover, good thermal stability was evidenced with the films remaining stable after annealing for 30 min at 1000 °C. Finally,

* Corresponding author.
E-mail address: holger.euchner@tuwien.ac.at (H. Euchner).

http://dx.doi.org/10.1016/j.actamat.2015.08.048
1359-6454/

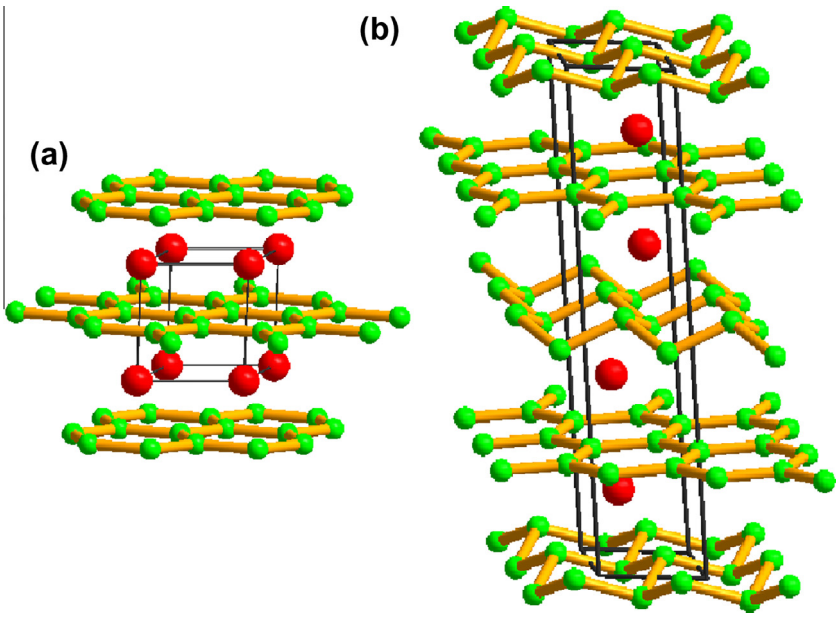

Fig. 1. Unit cell and layer structure of (a) AlB_2 and (b) WB_2 prototypes.

ab initio methods are used to explain the stabilization of α-$Ti_{1-x}W_xB_{2-z}$, evidencing the importance of point defects for PVD deposited materials. Indeed, in case of $Ti_{1-x}W_xB_2$ vacancies are crucial for the phase stability, which is fundamentally different to recent results on $Ti_xAl_{1-x}N$ [15]. This study classifies $Ti_{1-x}W_xB_2$ as a highly interesting material system and moreover underlines the huge impact vacancies may exert on the phase stability of PVD deposited coatings.

2. Experimental and computational methods

Ternary $Ti_{1-x}W_xB_{2-z}$ films have been deposited using an AJA Orion 5 lab-scale magnetron sputtering system. A 3-inch TiB_2 and a 2-inch WB_2 target (Plansee Composite Materials GmbH) were operated by an ENI RPG-100 and an ENI RPG-50 DC pulsed plasma generator with current controlled signal (pulse frequency of 150 kHz, pulse width of 2576 ns). After reaching a vacuum below 10^{-6} mbar, the single crystalline Si ((100) oriented) and polycrystalline Al_2O_3 substrates were heated to a temperature of 700 °C and then ion etched in Ar atmosphere (5×10^{-2} mbar). During deposition, the substrates, at floating potential, were kept at the constant temperature of 700 °C, while a working gas pressure (Ar) of 10^{-2} mbar was used. A deposition time in the order of ~180 min was chosen, resulting in thin films of about 2 µm thickness.

After dissolution with mineral acids, the chemical composition of the as-deposited thin films were determined by inductively coupled plasma atomic emission spectroscopy, also allowing for the determination of the boron content.

The structure of the thin films, deposited on Si and Al_2O_3 substrates, in the as-deposited state and after vacuum annealing at 1000 °C, was investigated by X-ray diffraction, using an Empyrean Panalytical diffractometer in grazing incidence geometry with an angle of incidence of $\omega = 2°$ (CuK_α, wave length $\lambda = 1.54$ Å). Moreover, scanning electron microscopy (SEM) was used to investigate the microstructure of the as-deposited coatings on the Si substrates.

Mechanical properties of the as-deposited coatings on Si substrates were obtained by using an ultra micro indentation system (UMIS), equipped with a Berkovich indenter. In order to minimize the substrate interference, loads within a range from 2 to 25 mN were applied. By analyzing the resulting load–displacement curves of the nanoindents after Oliver and Pharr [16], hardness and indentation modulus were determined.

To investigate the respective stability of vacancy-containing $Ti_{1-x}W_xB_2$ structures in α- and ω-modification, density functional theory (DFT) calculations have been conducted. The impact of vacancies on the phase stability of both structural modifications as well as the mechanical properties of the experimentally evidenced α-phase were investigated, using the Vienna Ab Initio Simulation Package (VASP) [17–19], applying the projector augmented waves method and the generalized gradient approximation (PAW–GGA).

In a first step, supercells of both structural modifications of $Ti_xW_{1-x}B_2$ were constructed. In case of α-$Ti_xW_{1-x}B_2$ a $2 \times 2 \times 4$ supercell with 48 atoms was investigated, while for ω-$Ti_xW_{1-x}B_2$ a $2 \times 2 \times 1$ supercell, also containing 48 atoms, was selected. Different chemical compositions were then realized by populating the metal sublattices with the corresponding Ti/W ratios, applying the special quasirandom structure (SQS) approach [20,21]. The SQS structures, obtained by making use of the atat package [21], were optimized with respect to lattice parameter and atom positions by applying the VASP code, using an energy cutoff of 600 eV and a $8 \times 8 \times 4$ Γ-centered k-point mesh. Both energy cutoff and k-point mesh were carefully chosen to ensure energy convergence within a few meV/at. Vacancy containing structures were then investigated by two different approaches. Starting from the defect-free supercells, vacancies were created by randomly removing either a boron or a metal (tungsten) atom, reducing the number of atoms per supercell to 47. In an additional approach, new 47 atoms SQS structures were created, by treating vacancies as further alloying elements. This second approach was applied to exclude effects, resulting from special local environments. For both scenarios, the resulting structures were again optimized, using the same settings as in case of the vacancy-free cells. To further investigate this behavior, an additional vacancy concentration was investigated by introducing two vacancies, a boron and a metal vacancy, into the supercells. Here again the second approach was applied, i.e. new SQS structures were created with vacancies treated as additional alloying elements. For this scenario such an approach is necessary, to avoid coincidental clustering of vacancies. The

resulting supercells, now containing 46 atoms, were again optimized with the above introduced settings. In addition, for comparison with results from nano-indentation and to investigate the impact of the different vacancy contents on the mechanical properties, we have calculated the Young's modulus of the binary phases α-$Ti_{1-y}B_{2-z}$ and α-$W_{1-y}B_{2-z}$ for various vacancy containing configurations. Here, again SQS structures in a $2 \times 2 \times 4$ supercell were created by treating vacancies as alloying elements, as described above. To extract the single crystal elastic constants, the universal linear independent coupling stress approach introduced by Yu et al. was applied [23]. Following this methodology, the relaxed supercells were deformed by six linearly independent strains, consequently yielding six different strain states. After optimizing the atomic positions of these six configurations, however, at fixed lattice constants, the remaining stresses were determined. The optimization of the strained configurations was carried out with the same settings as described above. By evaluating the stress–strain relation, the hexagonal single crystal elastic constants of the different binary compounds were determined from linear least square fits, using single value decomposition [23].

3. Results and discussion

Solid solutions of $Ti_{1-x}W_xB_2$ thin films could be synthesized for various Ti/W ratios, evidencing boron contents between ~65.4 and ~68.5 at.% (see Table 1). Due to the standard deviation of the boron content, amounting to up to ~4 at.%, in principle, both boron over- and under-stoichiometry is possible in our coatings.

XRD results highlight that all films are single phased and have crystallized – even at high tungsten content – in the AlB_2 structure type, see Fig. 2. Interestingly, TiB_2 as well as $Ti_{1-x}W_xB_2$ with low tungsten content exhibit pronounced (010) and (011) reflections, but no indication for (001). With further increasing tungsten content, the growth orientation changes and the (001) reflection becomes visible, which then is the only reflex present for tungsten contents of about 43% and 63 at.% on the metal sublattice.

With increasing tungsten content, both the (001) and the (011) reflections shift toward higher diffraction angles, whereas the (010) reflection remains at the position obtained for TiB_2. This indicates that replacing Ti by W results in decreasing lattice parameters along the c-axis, whereas the a- and b-axis remain nearly unchanged. Our $Ti_{1-x}W_xB_2$ thin films exhibit no changes in their XRD patterns upon 30-min vacuum annealing at 1000 °C, see Fig. 2(b), suggesting an outstanding thermal stability. All ternary $Ti_{1-x}W_xB_{2-z}$ thin films prepared exhibit a dense growth morphology as can be inferred from the SEM fracture cross sections in Fig. 3. At tungsten contents below 50 at.% on the metal sublattice, as exemplified for our $Ti_{0.86}W_{0.14}B_{2-z}$, $Ti_{0.67}W_{0.33}B_{2-z}$ and $Ti_{0.57}W_{0.43}B_{2-z}$ coatings in Fig. 3(a)–(c), the coatings show a rather equiaxed crystallization, while with increasing W content, a more columnar growth is present, see Fig. 3(d) and (e).

The indentation modulus of our films, as determined from nano-indentation, is depicted in Fig. 4 and shows an almost linear increase with the W content, from about ~350 for TiB_{2-z} to ~460 GPa for WB_{2-z}. For the hardness of our $Ti_{1-x}W_xB_2$ thin films, we find values above 30 GPa over the entire chemical composition range, while a pronounced maximum of about ~39 GPa is reached for W contents of 33 at.% and 43 at.% on the metal sublattice (see Fig. 4). As these two coatings differ in crystallographic orientation (see Fig. 2), the hardness increase can indeed be attributed to their chemical composition and the dense growth morphology. For both binary systems, TiB_2 and WB_2, the obtained values are in agreement with previous investigations (see e.g. [8,14]). However, both hardness and indentation modulus, have been shown to exhibit large variations, depending on the deposition conditions.

Ab intio calculations for $Ti_{1-x}W_xB_2$ predict the α-phase to only become energetically favorable, for Ti contents above ~50% [5] on the metal sublattice. Experimentally, we, however, clearly observe the α-structure type for the whole composition range. This is also in agreement with recent PVD studies by Jiang et al. [13], which report the deposition of α-WB_2. Due to PVD methods being known for the incorporation of point defects during the growth process, the formation of vacancies may provide a possible explanation for the stability of the α-structure, as also suggested for WB_2 [22].

The respective stability of α- and ω-$(Ti_xW_{1-x})_{1-y}B_{2-z}$ for different chemical and vacancy concentrations was studied in detail by comparing the energy of formation, E_f, of both structural modifications, following Eq. (1):

$$E_f = \frac{1}{\sum_i n_i}\left(E_{tot} - \sum_i n_i E_i\right) \quad (1)$$

here, E_{tot} and E_i denote the total energy of the compound and the elemental constituents, as determined from DFT, whereas n_i represents the number of atoms of species i. In case of $Ti_xW_{1-x}B_2$ the energy of formation describes the energy that is gained when an $Ti_xW_{1-x}B_2$ alloy is formed from α-Ti, bcc-W and α-boron.

In perfect agreement with previous results [22], we find WB_2 to be more stable in the ω-phase, whereas TiB_2 prefers the α-structure. The calculated total energy of both structural modifications and the lattice parameter of the experimentally evidenced α-phase of TiB_2 and WB_2 are denoted in Table 2. As expected from our XRD results, the a-axis lattice parameters of both binaries are almost identical. However, the lattice parameter along the c-axis of α-WB_2 is actually increased as compared to α-TiB_2. This is surprising, since an increasing lattice parameter for higher W contents would actually suggest a shift of the (001) reflection to lower diffraction angles, yet the opposite effect is observed in our XRD patterns. A possible explanation for these findings yields the incorporation of vacancies during the PVD process. As can also be inferred from Table 3, the c-axis lattice parameter of defected WB_2 is clearly decreasing with increasing vacancy content, whereas for TiB_2 only at high vacancy contents slight changes are observed. Therefore, the peak position in our XRD measurements strongly point toward an increased vacancy concentration in our thin films.

The striking impact that vacancies may exert on the phase stability of $Ti_xW_{1-x}B_2$ is presented in Fig. 5, showing the energy of formation for defect-free α- and ω- $Ti_xW_{1-x}B_2$ (Fig. 5(a)) as well as for metal and boron vacancy containing structures (Fig. 5(b) and (c)) with respect to the chemical composition. The vacancy containing structures exhibit the ω to α transition at significantly higher W contents.

In fact, while for the defect-free case the transition lies slightly above 50 at.% W on the metal sublattice, in agreement with recent predictions for larger supercells [5], both vacancy types (metal and boron vacancies), shift the transition clearly to the W-rich region to ~60 at.% W. Moreover, it is nicely visible that for both approaches

Table 1
Chemical composition of the as-deposited $Ti_xW_{1-x}B_2$ thin films. The sample names give the composition of the metal sublattice.

Sample	Ti (at.%)	W (at.%)	B (at.%)
Ti*	33.3		66.7
$Ti_{0.86}W_{0.14}$	28.3 ± 0.2	4.5 ± 0.1	67.3 ± 0.3
$Ti_{0.67}W_{0.33}$	22.2 ± 1.6	10.7 ± 0.7	67.1 ± 4.4
$Ti_{0.57}W_{0.43}$	18.0 ± 0.4	13.5 ± 0.3	68.5 ± 2.7
$Ti_{0.37}W_{0.63}$	12.8 ± 0.2	21.9 ± 0.4	65.2 ± 3.1
W		34.6 ± 0.2	65.4 ± 4.2

* Target composition.

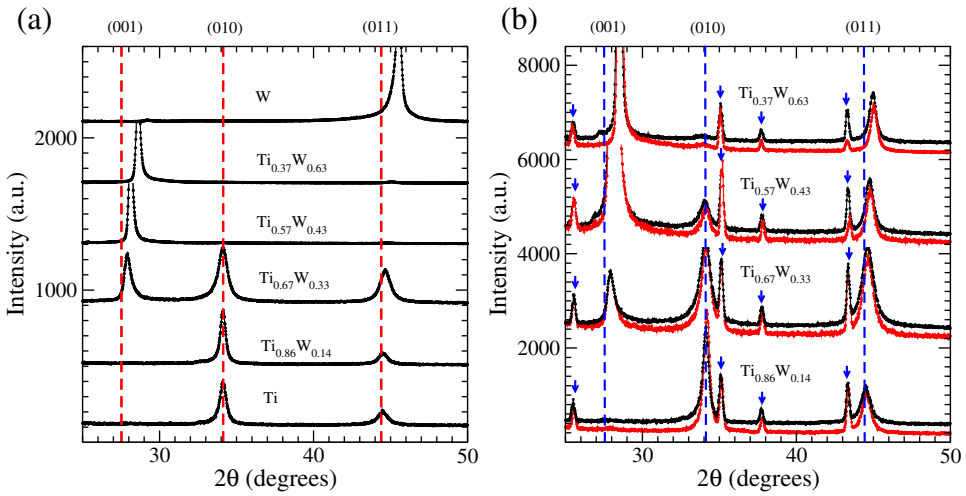

Fig. 2. Diffraction pattern (grazing incidence) of $Ti_xW_{1-x}B_2$ thin films deposited on Si substrates (a) and on polycrystalline Al_2O_3 substrates before (black) and after (red) annealing at 1000 °C (b). The vertical, dashed lines indicate the standard positions of bulk TiB_2. The small arrows (b) indicate peaks stemming from the Al_2O_3 substrates. (For interpretation of the references to color in this figure legend, the reader is referred to the web version of this article.)

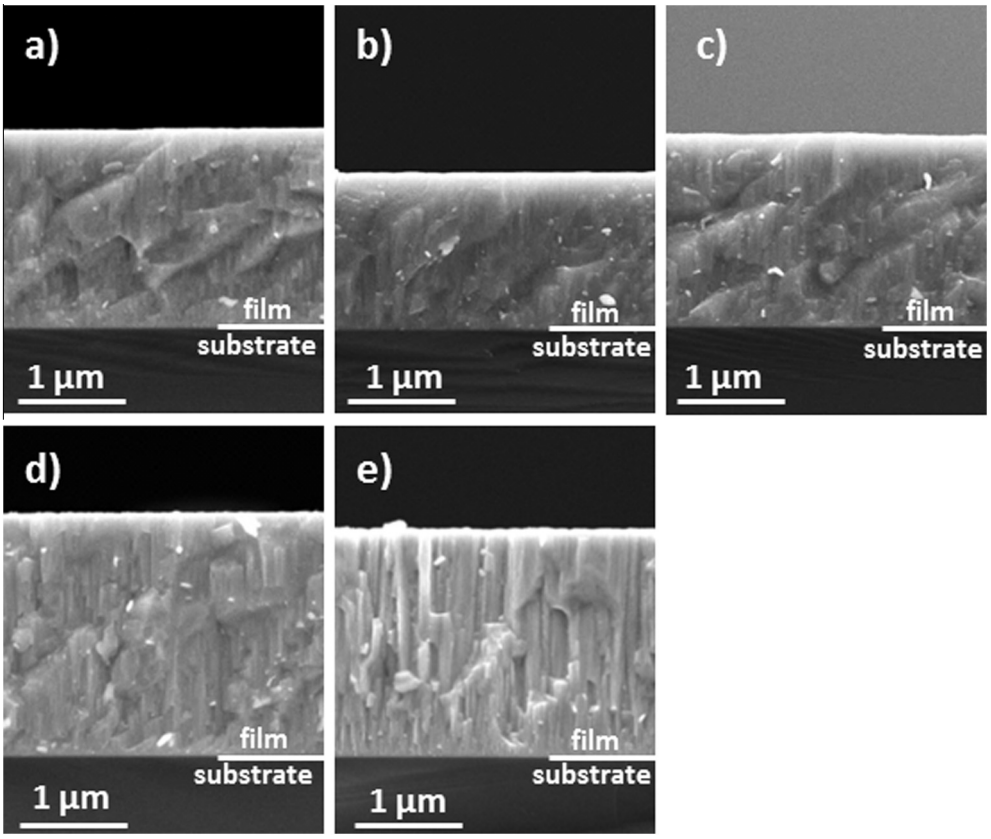

Fig. 3. SEM fracture cross section of $Ti_{0.86}W_{0.14}B_{2-z}$ (a), $Ti_{0.67}W_{0.33}B_{2-z}$ (b), $Ti_{0.57}W_{0.43}B_{2-z}$ (c), $Ti_{0.37}W_{0.63}B_{2-z}$ (d) and WB_{2-z} (e) thin films on Si substrates.

(open and filled symbols in Fig. 5), the results are almost identical, thus excluding artificial effects due to special vacancy configurations. Strikingly, structures containing both vacancy types (i.e. a boron and a metal vacancy in one supercell) exhibit an even more pronounced shift of the ω to α transition to higher W-contents, pushing it even slightly above a W content of 80 at.% on the metal sublattice (see Fig. 6).

The changing transition concentration emphasizes the strong impact that vacancies may exert on the phase stability. From the dashed, vertical lines in Figs. 5 and 6, which roughly mark the upper and lower limit of the transition regime, the changing transition composition is nicely visible. Interestingly, the shape of the energy of formation curves does not significantly change for the different vacancy concentrations. The above discussion had its focus on the energy of formation, thus neglecting the impact of entropic contributions. This is justified, since the configurational entropy depends only on the chemical composition, such that it is equivalent for both structural modifications of $Ti_xW_{1-x}B_2$.

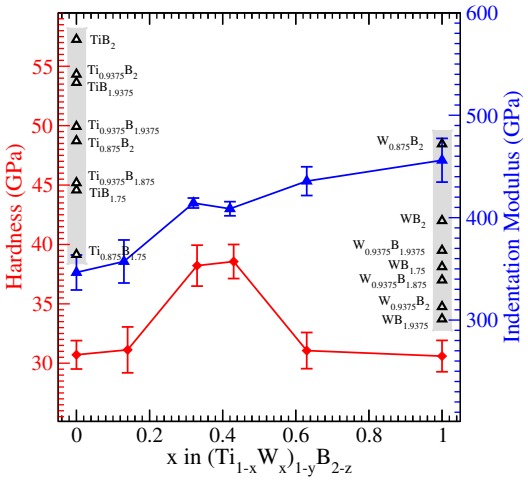

Fig. 4. Hardness (red diamonds) and indentation modulus (blue triangles) of $Ti_xW_{1-x}B_2$ thin films depicted with respect to the W concentration. The calculated Young's moduli of $Ti_{1-y}B_{2-z}$ and $W_{1-y}B_{2-z}$ for different vacancy contents on metal and boron sublattice are shown as open triangles. (For interpretation of the references to color in this figure legend, the reader is referred to the web version of this article.)

Vibrational entropy on the other hand may differ for both modifications, yet due to the structural similarity differences may only become significant at elevated temperatures.

Finally, by comparing vacancy-containing and defect-free structures, it is possible to extract the vacancy formation energy:

$$E_f^{vac}[B] = \frac{n}{3}\left(E_{tot}[Ti_{1-x}W_xB_2] - E_{tot}[Ti_{1-x}W_xB_{2-z}] - zE_{tot}[B]\right) \quad (2)$$

with n the total number of atoms, whereas $E_{tot}[Ti_{1-x}W_xB_2]$ and $E_{tot}[Ti_{1-x}W_xB_{2-z}$ denote the total energy of a formula unit of defect-free and defected $Ti_{1-x}W_xB_2$, while $E_{tot}[B]$ is the total energy of α-boron.

For metal vacancies, the formalism becomes a bit more demanding since one has to account for a changing Ti/W ratio on the metal sublattice. The formation energy of a defect then takes the following appearance:

$$E_f^{vac}[M] = \frac{n}{3}\Big(E_{tot}[Ti_{1-x}W_xB_2] - E_{tot}[(Ti_{1-x}W_x)_{1-y}B_2] - y[[(1-x)E_{tot}[Ti] + xE_{tot}[W]]\Big) \quad (3)$$

with n the total number of atoms, whereas $E_{tot}[Ti_{1-x}W_xB_2]$ and $E_{tot}[Ti_{1-x}W_xB_{2-z}]$ denote the total energy of a formula unit of defect-free and defected $Ti_{1-x}W_xB_2$, while $E_{tot}[B]$ is the total energy of α-boron. Finally, $1-x$ $E_{tot}[Ti]$ and x $E_{tot}[W]$ sum up to the total energy of a pseudo-atom, consisting of α-Ti and bcc-W, weighted by their stoichiometric abundances. The introduction of this pseudo-atom ensures a non-changing stoichiometry when comparing deficient and non-deficient structure as it would be the case for the creation of a vacancy in a macroscopic system. Using the above equations, the formation energies for metal and boron vacancies in α- and ω-$Ti_xW_{1-x}B_2$ were determined. Due to the limited supercell sizes in our calculations, the stoichiometry on the metal sublattice of metal deficient and vacancy-free structures is slightly different.

Table 2
Total energies for TiB_2 and WB_2 in the respective structural modification.

Structure type	AlB_2 (α) E_{tot}(eV/at)	WB_2 (ω) E_{tot}(eV/at)
TiB_2	−8.103	−7.712
WB_2	−8.778	−9.038

Therefore, to access the correct vacancy formation energies for the case of metal vacancies, we have interpolated the energies of the defected crystal over the whole composition range, using a third order polynomial fit. Thus the energy of perfect structures and defected structure with the same stoichiometry on the metal sublattice could be extracted. The resulting vacancy formation energies are depicted in Fig. 7. Surprisingly, with increasing W content, vacancies get less unfavorable in the α-phase, and for high W contents the formation of vacancies is energetically even favorable. The formation of vacancies in the ω-phase, on the other hand, remains energetically unfavorable over the entire composition range. Thus, also from an energetical point of view, the experimentally evidenced α-phase is likely to contain a rather increased vacancy content. Due to the additional disorder, which is introduced by the presence of vacancies, the configurational entropy is increased and therefore entropy even further stabilizes the defected α-phase.

Furthermore, the impact of vacancies on the mechanical properties of the binary α-phase was investigated. For this purpose, the single crystal elastic constants of different binary α-$Ti_{1-y}B_{2-z}$ and α-$W_{1-y}B_{2-z}$ phases were determined as described above. Before extracting the Voigt–Reuss–Hill average of bulk modulus (B_{vrh}) and shear modulus (G_{vrh}) [24,25], the different binaries were investigated for mechanical stability and could be shown to fulfill the stability criterion for hexagonal crystals [24]. Then, to enable a comparison with experimental data, the Young's moduli were determined following Eq. (4):

$$Y_{vrh} = (9B_{vrh}G_{vrh})/(3B_{vrh} + G_{vrh}) \quad (4)$$

In addition to the indentation modulus of α-$Ti_{1-x}W_xB_{2-z}$ as obtained from nano-indentation, Fig. 4 depicts the calculated Young's moduli of binary phases with different vacancy contents. Surprisingly, for both α-$Ti_{1-y}B_{2-z}$ and α-$W_{1-y}B_{2-z}$, vacancies significantly influence the elastic properties. In fact, for α-$Ti_{1-y}B_{2-z}$ the calculated Young's modulus lies between ~570 and ~360 GPa for TiB_2 and $Ti_{0.875}B_{1.75}$, respectively. It is noteworthy that these two structures both evidence a B:Ti ratio of 2:1. For α-$W_{1-y}B_{2-z}$, the Young's modulus ranges from ~300 GPa for $WB_{1.9375}$ to ~480 GPa for $W_{0.875}B_2$. Hence, the mechanical properties of the binaries are highly sensitive to the vacancy concentration, which may also serve as an explanation for the large variation of these properties in literature. However, while in case of α-$Ti_{1-y}B_{2-z}$ vacancies result in a reduction of Young's modulus, for α-$W_{1-y}B_{2-z}$ the maximum value is found for a structure containing vacancies on the metal sublattice. This indicates that vacancies may even result in a strengthening of α-$W_{1-y}B_{2-z}$.

4. Summary and conclusion

Sputter deposited $Ti_xW_{1-x}B_{2-z}$ thin films were, for the whole composition range, shown to crystallize in the AlB_2 structure type.

Table 3
c-axis lattice parameters for binary α-TiB_2 and α-WB_2 with different vacancy concentrations.

	MB_2 (Å)	$MB_{1.9375}$ (Å)	$M_{0.9375}B_2$ (Å)	$M_{0.9375}B_{1.9375}$	$M_{0.9375}B_{1.875}$ (Å)	$M_{0.875}B_{1.75}$
M = Ti	3.23	3.23	3.23	3.23	3.22	3.19
M = W	3.40	3.32	3.31	3.24	3.23	3.11

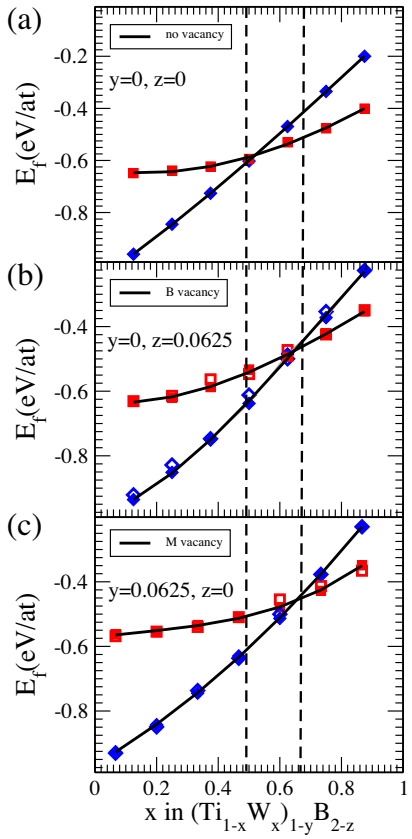

Fig. 5. E_f of defect-free (a), boron deficient (b) and metal deficient (c) $(Ti_xW_{1-x})_{1-y}B_{2-z}$ for 48 atom supercells with no (a) and one (b,c) vacancies are shown. The α-phase is depicted as blue diamonds, whereas the ω-phase is represented by red squares. Filled symbols are obtained by treating vacancies as additional alloying element, empty symbols by randomly removing an atom from the defect-free structures. Black curves are third order polynomial fits to the data.

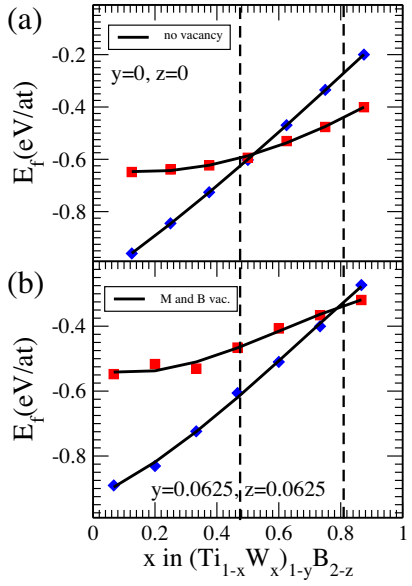

Fig. 6. Comparison of E_f for defect-free $Ti_xW_{1-x}B_2$ (a) and defected $(Ti_xW_{1-x})_{1-y}B_{2-z}$ with vacancies on metal and boron sublattice. Results corresponding to a 48 atoms supercell without (a) and with two (b) vacancies are shown. The α-phase is depicted as blue diamonds, whereas the ω-phase is represented by red squares. Black curves are third order polynomial fits to the data. (For interpretation of the references to color in this figure legend, the reader is referred to the web version of this article.)

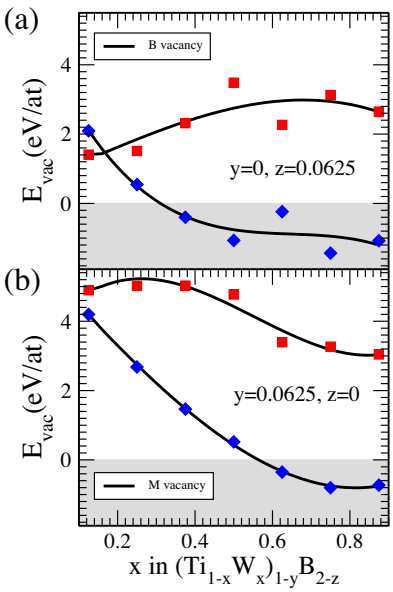

Fig. 7. Formation energy for boron (a) and metal (b) vacancies in α- and ω- $(Ti_xW_{1-x})_{1-y}B_{2-z}$. The α-phase is depicted in blue, the ω-phase in red. The gray shaded area indicates negative vacancy formation energies. (For interpretation of the references to color in this figure legend, the reader is referred to the web version of this article.)

Evidencing high hardness of up to almost 40 GPa, together with a good thermal stability, this material system is a promising candidate for industrial application. Using ab initio methods, we have provided vacancies as possible explanation for the stabilization of the α-phase in this ternary system. Our calculations clearly evidence that vacancies result in a shift of the α to ω transition toward lower Ti contents. Placing one vacancy on metal and boron sublattice, respectively, results in shifting the transition to a Ti content of about 20 at.%. Since two vacancies in a 48 atom supercell correspond to a vacancy concentration of about 4 at.% this scenario is certainly realistic and it is even likely that higher vacancy concentration occur in PVD deposited coatings. Moreover, the fact that the computed lattice parameter of vacancy-free α-WB_2 is increased as compared to α-TiB_2, whereas diffraction data make us expect a decrease, also strongly points to a significant vacancy concentration in our coatings. Finally, the Young's modulus of the different binary phases showed a large variation with respect to the vacancy content. A fact, which may hold as explanation for the large spread of experimentally determined hardness and indentation modulus of TiB_2 thin films. Our experimental and computational results strongly emphasize the importance of point defects for phase stability and mechanical properties of PVD deposited thin films, a fact which is often neglected when these systems are modeled using ab-initio calculations.

Acknowledgment

We thank the Vienna Scientific Cluster for the attribution of computation time and the X-ray center of TU Wien for beam time. The present study was partly held within START Project (Y371) of the Austrian Science Fund (FWF).

References

[1] A. Hörling, L. Hultman, M. Odén, J. Sjölén, L. Karlsson, Mechanical properties and machining performance of $Ti_{1-x}Al_xN$-coated cutting tools, Surf. Coatings Technol. 191 (2–3) (2005) 384–392.
[2] P.H. Mayrhofer, L. Hultman, J.M. Schneider, Spinodal decomposition of cubic $Ti_{1-x}Al_xN$: comparison between experiments and modeling, Int. J. Mat. Res. 98 (11) (2007) 1054–1059.

[3] R. Rachbauer, S. Massl, E. Stergar, Decomposition pathways in age hardening of Ti-Al-N films, J. Appl. Phys. 110 (2011) 023515.
[4] M. Schlögl, C. Kirchlechner, J. Paulitsch, J. Keckes, P. Mayrhofer, Effects of structure and interfaces on fracture toughness of CrN/AlN multilayer coatings, Scr. Mater. 68 (12) (2013) 917–920.
[5] H. Euchner, P. Mayrhofer, Designing thin film materials — Ternary borides from first principles, Thin Solid Films 583 (2015) 46–49.
[6] O. Knotek, Industrial deposition of binary, ternary, and quaternary nitrides of titanium, zirconium, and aluminum, J. Vac. Sci. Technol. A Vac. Surf. Film. 5 (4) (1987) 2173.
[7] P. Losbichler, C. Mitterer, Non-reactively sputtered TiN and TiB_2 films: influence of activation energy on film growth, Surf. Coat. Technol. 97 (1-3) (1997) 567–573.
[8] E. Kelesoglu, C. Mitterer, M. Kazmanli, M. Ürgen, Microstructure and properties of nitride and diboride hard coatings deposited under intense mild-energy ion bombardment, Surf. Coat. Technol. 116-119 (1999) 133–140.
[9] P.H. Mayrhofer, C. Mitterer, J.G. Wen, J.E. Greene, I. Petrov, Self-organized nanocolumnar structure in superhard TiB_2 thin films, Appl. Phys. Lett. 86 (13) (2005) 131909.
[10] W. Hofmann, W. Janiche, Der Strukturtyp von Aluminiumborid (AlB_2), Naturwissenschaften 23 (50) (1935). 851–851.
[11] M. Frotscher, W. Klein, J. Bauer, M_2B_5 or M_2B_4 reinvestigation of the Mo/B and W/B system, Zeitschrift für anorganische und allgemeine Chemie 633 (15) (2007) 2626–2630.
[12] H.P. Woods, F.E. Wawner, B.G. Fox, Tungsten diboride: preparation and structure, Science 151 (3706) (1966) 75.
[13] C. Jiang, Z. Pei, Y. Liu, J. Xiao, J. Gong, C. Sun, Preparation and characterization of superhard AlB_2 type WB_2 nanocomposite coatings, Phys. Status Solidi 210 (6) (2013) 1221–1227.
[14] Y. Liu, C. Jiang, Z. Pei, H. Lei, J. Gong, C. Sun, Microstructure and properties of AlB_2-type WB_2 thin films deposited by direct-current magnetron sputtering, Surf. Coat. Technol. 245 (2014) 108–116.
[15] H. Euchner, P. Mayrhofer, Vacancy-dependent stability of cubic and wurtzite $Ti_{1-x}Al_xN$, Surf. Coat. Technol. 275 (2015) 214–218.
[16] W. Oliver, G. Pharr, Measurement of hardness and elastic modulus by instrumented indentation: advances in understanding and refinements to methodology, J. Mater. Res. 19 (01) (2011) 3–20.
[17] G. Kresse, J. Furthmüller, Efficiency of ab-initio total energy calculations for metals and semiconductors using a plane-wave basis set, Comput. Mater. Sci. 6 (1) (1996) 15–50.
[18] G. Kresse, Efficient iterative schemes for ab initio total-energy calculations using a plane-wave basis set, Phys. Rev. B 54 (16) (1996) 11169–11186.
[19] G. Kresse, J. Hafner, Ab-initio molecular dynamics for liquid metals, Phys. Rev. B 47 (1) (1993) 558–561.
[20] A. Zunger, S.-H. Wei, L. Ferreira, J. Bernard, Special quasirandom structures, Phys. Rev. Lett. 65 (3) (1990) 353–356.
[21] A. van de Walle, P. Tiwary, M. de Jong, Efficient stochastic generation of special quasirandom structures, Calphad 42 (2013) 13–18.
[22] W. Hayami, A. Momozawa, S. Otani, Effect of defects in the formation of AlB_2-type WB_2 and MoB_2, Inorg. Chem. 52 (13) (2013) 7573–7577.
[23] R. Yu, J. Zhu, H. Ye, Calculations of single-crystal elastic constants made simple, Comput. Phys. Commun. 181 (3) (2010) 671–675.
[24] H.M. Ledbetter, Elastic properties of zinc – a compilation and a review, J. Phys. Chem. Ref. Data 6 (4) (1977) 1181–1203.
[25] R. Hill, The elastic behaviour of a crystalline aggregate, Proc. Phys. Soc. Sect. A 65 (5) (1952) 349–354.